iScience

Article

Mesenchymal Hippo signaling regulates intestinal homeostasis in adult mice

Graphical abstract

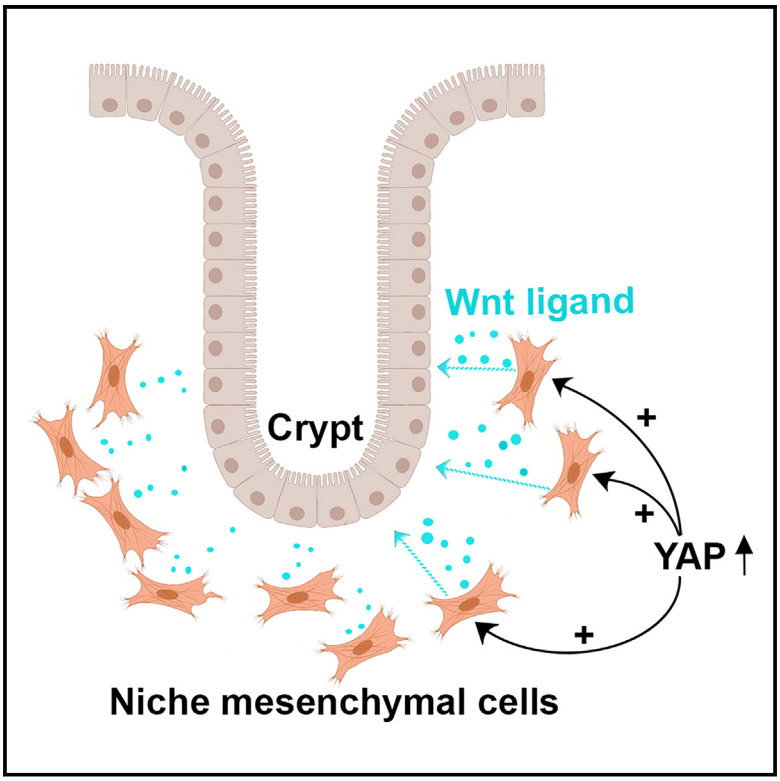

Authors

Kyvan Dang, Alka Singh, Xin Chen, ..., Y. Tony Ip, Xu Wu, Junhao Mao

Correspondence

junhao.mao@umassmed.edu

In brief

Molecular biology; Cell biology

Highlights

- Hippo signaling plays a critical role in the niche-forming Gli1$^+$ mesenchymal cells
- Mesenchymal Hippo pathway regulates the intestinal epithelial-mesenchymal crosstalk
- YAP is upregulated in the mesenchyme during intestinal injury
- Stromal YAP activation promotes intestinal epithelial regeneration

Dang et al., 2025, iScience *28*, 111847
February 21, 2025
https://doi.org/10.1016/j.isci.2025.111847

CellPress

iScience

CellPress
OPEN ACCESS

Article

Mesenchymal Hippo signaling regulates intestinal homeostasis in adult mice

Kyvan Dang,[1] Alka Singh,[1] Xin Chen,[1] Jennifer L. Cotton,[1] Susu Guo,[1] Xiaodi Hu,[1] Zhipeng Tao,[2,3] Haibo Liu,[1] Lihua J. Zhu,[1] Y. Tony Ip,[4] Xu Wu,[2] and Junhao Mao[1,5,*]

[1]Department of Molecular, Cell and Cancer Biology, University of Massachusetts Chan Medical School, Worcester, MA 01605, USA
[2]Cutaneous Biology Research Center, Massachusetts General Hospital, Harvard Medical School, Charlestown, MA, USA
[3]Department of Nutrition and Food Sciences, Texas Woman's University, Denton, TX 76204, USA
[4]Program in Molecular Medicine, University of Massachusetts Chan Medical School, Worcester, MA 01605, USA
[5]Lead contact
*Correspondence: junhao.mao@umassmed.edu
https://doi.org/10.1016/j.isci.2025.111847

SUMMARY

Intestinal homeostasis is tightly regulated by the reciprocal interaction between the gut epithelium and adjacent mesenchyme. The Hippo pathway is intimately associated with intestinal epithelial homeostasis and regeneration; however, its role in postnatal gut mesenchyme remains poorly defined. Here, we find that removal of the core Hippo kinases Lats1/2 or activation of YAP in adult intestinal smooth muscle layers has largely no effect; however, Hippo-YAP signaling in the niche-forming Gli1+ mesenchymal cells plays intrinsic roles in regulating intestinal homeostasis. We find that Lats1/2 deletion drives robust mesenchymal over-proliferation, and YAP activation in Gli1+ pericryptal cells disrupts the intestinal epithelial-mesenchymal crosstalk via promoting Wnt ligand production. We show that YAP is upregulated in the stroma during dextran sodium sulfate (DSS)-induced injury, and mesenchymal YAP activation facilitates intestinal epithelial regeneration. Altogether, our data suggest an important role for mesenchymal Hippo-YAP signaling in the stem cell niche during intestinal homeostasis and pathogenesis.

INTRODUCTION

The mammalian gastrointestinal tract comprises the endodermis-derived epithelium surrounded by adjacent mesoderm-derived mesenchyme. Continuous crosstalks between these two tissue layers are critical for intestinal development and postnatal homeostasis.[1] However, compared to the intestinal epithelium, the genetic and molecular mechanisms governing mesenchymal growth, differentiation, and homeostasis are under-studied and poorly understood. It is known that mesenchymal/stromal dysfunction is closely associated with human digestive tract diseases.[1] Recent studies have also demonstrated that subepithelial mesenchymal cells form the essential Wnt-secreting niche needed to sustain intestinal epithelial stem cells in the crypt,[2,3] therefore playing a pivotal role in controlling intestinal homeostasis.

The Hippo pathway, originally identified in *Drosophila* as an organ size control pathway, consists of a core kinase cascade, Mst1/2 and Lats1/2, which phosphorylate and inactivate the transcriptional co-activators YAP and TAZ. Upon upstream Hippo signaling inactivation, YAP and TAZ translocate into the nucleus and interact with the TEAD family of transcription factors, thereby inducing downstream gene expression.[4–10] Work from us and many others demonstrated a critical requirement for epithelial Hippo signaling in intestinal stem cell maintenance and regeneration.[6,11–16] Furthermore, our prior work also uncovered the previously unappreciated requirement of YAP/TAZ in the embryonic gut mesenchyme, linking the Hippo-YAP pathway to intestinal mesenchymal homeostasis.[17] We found that YAP and TAZ function as a molecular switch to coordinate mesenchymal growth and patterning in the developing gut.[17] However, the precise role of Hippo-YAP signaling in the stromal compartment of the adult intestine remains largely unknown.

In this study, we explored the function of stromal Lats1/2, the core Hippo kinases, during intestinal homeostasis, focusing on their roles in the subepithelial mesenchymal populations within the stem cell niche. We found that Hippo signaling controls the proliferation of the Gli1$^+$ niche-forming mesenchymal cells and regulates intestinal epithelial-mesenchymal crosstalk. Our data also show that YAP activation in the mesenchyme promotes intestinal epithelial regeneration following injury.

RESULTS

Hippo-YAP signaling status in postnatal intestinal mesenchyme

To explore mesenchymal Hippo-YAP signaling during intestinal homeostasis, we first examined the expression of YAP/TAZ in the adult intestine. Immunohistochemical (IHC) staining and immunoblotting for YAP/TAZ showed that YAP and TAZ were highly expressed in the intestinal mesenchyme in comparison to the intestinal epithelium (Figures 1A and 1B), which is

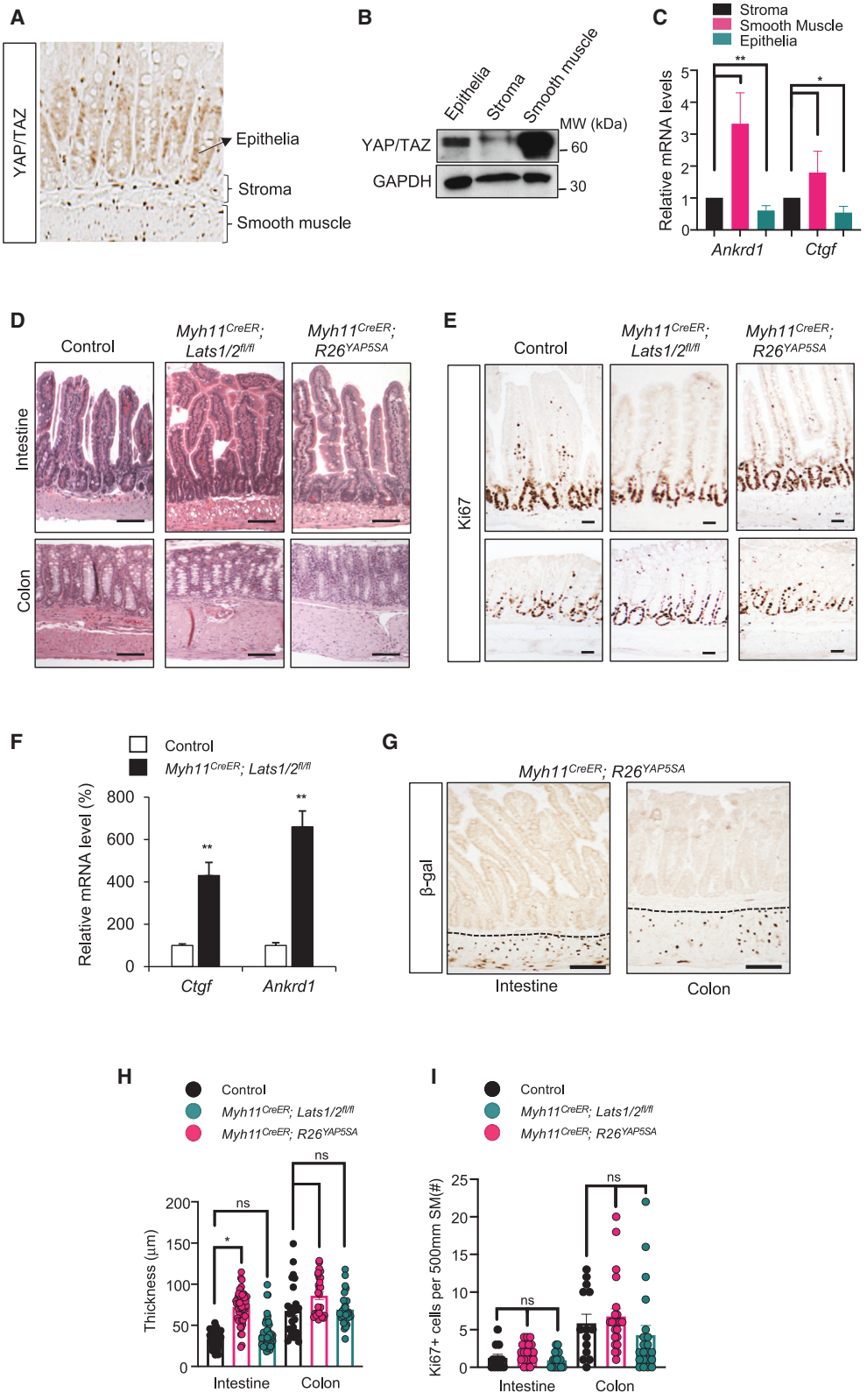

(legend on next page)

consistent with our prior report of higher YAP/TAZ activity in the mesenchyme of embryonic gut.[17] Among the postnatal mesenchymal compartments, we found that the YAP/TAZ levels were significantly higher in the outer smooth muscle layers than those in the subepithelial mesenchymal cells (Figure 1B), which is further confirmed by our quantitative reverse-transcription PCR (qRT-PCR) analysis of the transcription of *bona fide* YAP/TAZ target genes, *Ctgf* and *Ankrd1*, in these cells (Figure 1C). These data suggested that the differentiated smooth muscle cells have higher baseline YAP/TAZ activation than the subepithelial mesenchymal populations.

Disruption of Hippo-YAP signaling in intestinal smooth muscle

To investigate the role of Hippo-YAP signaling in adult intestinal smooth muscle cells, we either crossed the floxed *Lats1/2* alleles (*Lats1/2* $^{fL/fL}$)[18] or the conditional active YAP allele, *R26*^{YAP5SA}[17] to smooth muscle cell-specific *Myh11*^{CreER}.[19] Recombination was induced in adult animals via tamoxifen intraperitoneal injections at post-natal day 30 (P30). In the *R26*^{YAP5SA} allele we generated, YAP5SA, a constitutively active form of YAP that has five canonical LATS phosphorylation sites mutated from serine to alanine[20] and carries a C-terminal IRES-nuclear β-galactosidase tag, was targeted into the *Rosa26* locus.[17] We found surprisingly that Lats1/2 deletion or constitutively active YAP expression in the smooth muscle layers did not significantly change the overall intestinal morphology, even 80 days following tamoxifen induction in both *Myh11*^{CreER}*; Lats1/2* $^{fL/fL}$ and *Myh11*^{CreER}*; R26*^{YAP5SA} mutants (Figure 1D). Our qRT-PCR analysis detected the elevated expression levels of YAP/TAZ targets *Ctgf* and *Ankrd1*, confirming YAP/TAZ activation in Lats1/2-mutant animals (Figure 1F). IHC analysis of β-galactosidase in *Myh11*^{CreER}*; R26*^{YAP5SA} mutants following tamoxifen injection showed nuclear signal exclusively in the smooth muscles of both intestine and colon, indicating transgenic YAP^{5SA} expression (Figure 1G).

Our analyses further revealed that Lats1/2 deletion or YAP activation in gut smooth muscle cells could not induce significant proliferation, measured by Ki67 staining (Figures 1E and 1H), and there is little or no change in smooth muscle thickness between control and mutant animals (Figure 1I). In addition, we did not observe significant changes in the growth and differentiation of the intestinal epithelia in mutant animals (Figure S1). Although we could not observe mutant animals beyond 90 days after tamoxifen injection due to the overall health deterioration of mutant mice, including severe skin lesions, these data suggested that disruption of Hippo-YAP signaling via Lats1/2 deletion or constitutive YAP activation did not generate an obvious phenotype in the terminally differentiated intestinal smooth muscle cells.

Lats1/2 deletion and YAP activation drive overproliferation of niche-forming Gli1+ mesenchymal cells

We next explored Hippo-YAP function in the subepithelial compartment of the intestinal mesenchyme. Our effort was focused on the critical mesenchymal populations that form the intestinal stem cell niche. Gli1-expressing cells have recently been identified as one of the major subepithelial mesenchymal populations serving as a major source of Wnt ligands, and these pericryptal Gli+ cells have been demonstrated to be essential for the maintenance of the stem cell niche and intestinal homeostasis.[21]

To determine the role of Hippo-YAP signaling in this critical niche-forming mesenchymal cell population, we crossed the *Gli1*^{CreER}[22]-inducible Cre mice to the floxed *Lats1/2* alleles or *R26*^{YAP5SA}. The mutant mice were treated with tamoxifen via intraperitoneal injection at P30 to induce Cre-mediated recombination. At 2 months following tamoxifen induction, pronounced overgrowths were detected in the small intestine and colon of the mutant animals (Figures 2A and S2). These overgrowth areas exhibited disturbed epithelial architecture and drastic mesenchymal expansion (Figures 2A and S2). In the *Gli1*^{CreER}*; Lats1/2* $^{fL/fL}$ mice, IHC of YAP and TAZ showed nuclear YAP/TAZ staining within the expanded mesenchyme (Figure 2B), indicating YAP/TAZ activation induced by Lats1/2 deletion. In *Gli1*^{CreER}; *R26*^{YAP5SA} mice, IHC of nuclear β-galactosidase demonstrated that YAP5SA transgene expression in the overgrowth regions occurred exclusively in the vimentin-expressing mesenchymal cells (Figures 2C and S2). Furthermore, immunofluorescence staining of YPA and vimentin demonstrated the localization of nuclear YAP in vimentin^{+} cells in the mesenchymal overgrowths detected in the *Gli1*^{CreER}*; Lats1/2* $^{fL/fL}$ mice (Figure 2D). In comparison to the control pericryptal mesenchyme cells, the mesenchymal cells carrying Lats1/2 deletion or YAP5SA expression were also highly proliferative, measured by Ki67 or PCNA staining (Figures 2E, 2F, and S2). Together, these data showed that YAP/TAZ activation can drive

Figure 1. Disruption of Hippo-YAP signaling in adult intestinal smooth muscle

(A) Immunohistochemistry of YAP/TAZ in control intestine, showing YAP/TAZ staining in intestinal epithelia, subepithelial stroma, and smooth muscle layers.

(B) Immunoblot analysis of YAP/TAZ and GAPDH in intestinal epithelia, stroma, and smooth muscle.

(C) Real-time PCR analysis showing relative mRNA levels of *Ankrd1* and *Ctgf* mRNA levels in intestinal stroma, smooth muscle, and epithelia.

(D) Histology of intestine and colon of control, *Myh11*^{CreER}*; R26*^{YAP5SA}, and *Myh11*^{CreER}*; Lats1/2* $^{fL/fL}$ animals. Scale bar, 50 μm.

(E) Immunohistochemical Ki67 staining in intestine and colon of control, *Myh11*^{CreER}*; R26*^{YAP5SA}, and *Myh11*^{CreER}*; Lats1/2* $^{fL/fL}$ animals. Scale bar, 50 μm.

(F) Real-time PCR analysis of *Ctgf* and *Ankrd1* mRNA levels in control and *Myh11*^{CreER}*; Lats1/2* $^{fL/fL}$ mutant smooth muscle cells.

(G) Immunohistochemistry of β-galactosidase (β-gal) in the intestine and colon of *Myh11*^{CreER}*; R26*^{YAP5SA} animals. Stroma-smooth muscle boundary is indicated by dashed line. Scale bar, 50 μm.

(H) Quantification of thickness of smooth muscle layer in the intestine and colon of control, *Myh11*^{CreER}*; R26*^{YAP5SA}, and *Myh11*^{CreER}*; Lats1/2* $^{fL/fL}$ animals. $n = 27$ per group per anatomical location.

(I) Quantification of Ki67^{+} smooth muscle cells in the smooth muscle layer in the intestine and colon of WT, *Myh11*^{CreER}*; R26*^{YAP5SA}, and *Myh11*^{CreER}*; Lats1/2* $^{fL/fL}$ animals.

Data are mean ± SEM, $^{*}p < 0.05$, $^{**}p < 0.01$, ns: not significant.

See also Figure S1.

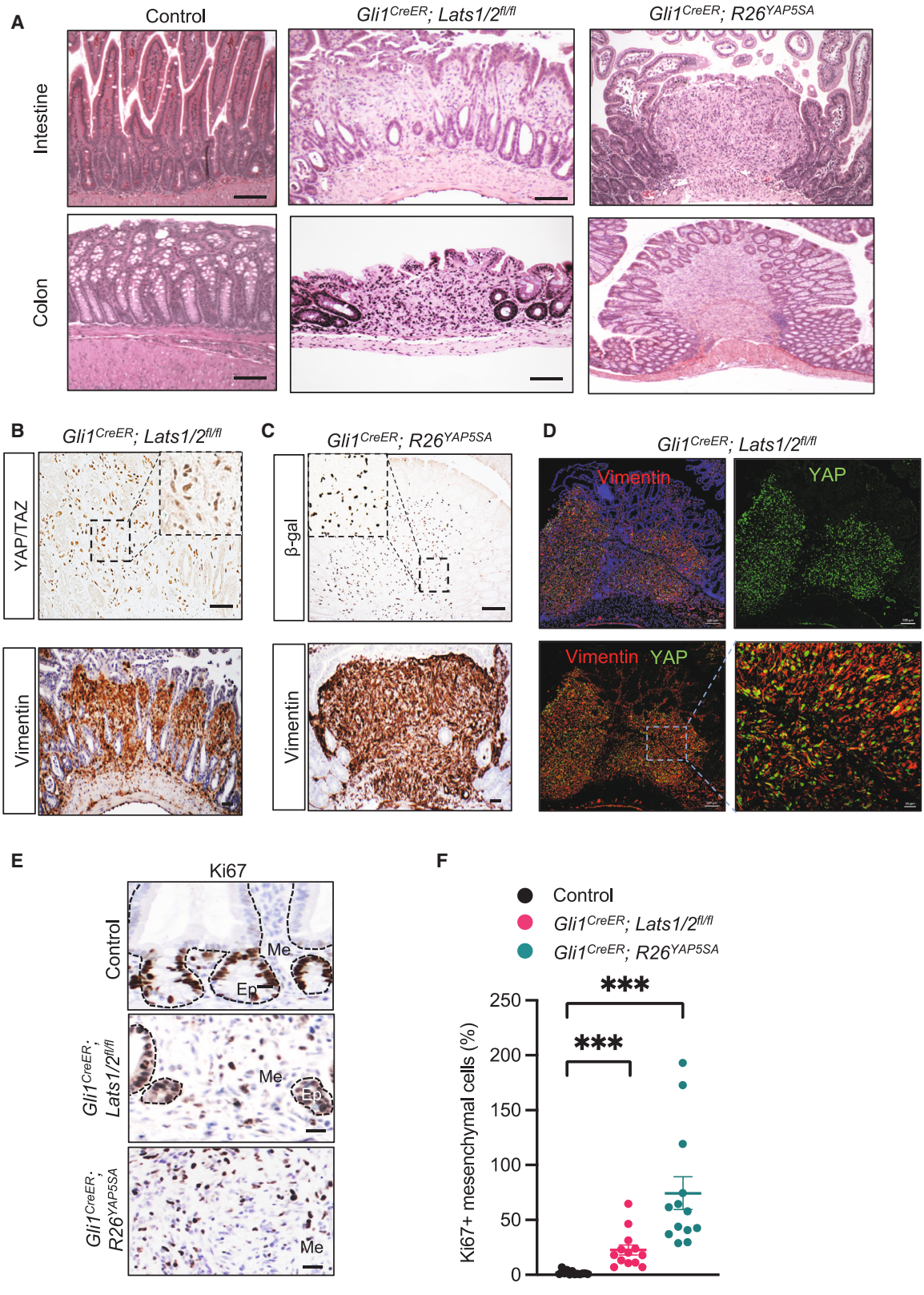

(legend on next page)

over-proliferation of Gli1-expressing subepithelial mesenchymal cells and induce intestinal overgrowth.

SMA downregulation in mesenchymal overgrowth induced by Hippo inhibition

Previous studies showed that the Gli1-expressing stromal cells located near the bases of intestinal crypts exhibit the characteristics of mesenchymal progenitors that are capable of undergoing differentiation of several lineages, including smooth muscle actin (SMA)-expressing myofibroblasts.[21] Interestingly, we noticed that SMA expression was markedly reduced in the mesenchymal overgrowths induced by *Gli1*^{CreER}-induced YAP activation or Lats1/2 deletion when compared to the stromal compartment in control animals (Figure 3A). Our qRT-PCR analysis also showed that SMA transcription was downregulated in the subepithelial stroma isolated from *Gli1*^{CreER}; *Lats1/2*$^{fL/fL}$ and *Gli1*^{CreER}; *R26*^{YAP5SA} mice (Figure 3B). These data raised an intriguing possibility that YAP/TAZ may be involved in regulating SMA expression or the differentiation potential of Gli1$^+$ mesenchymal cells.

To further explore this phenotype, we generated the *Gli1*^{CreER}; *R26*$^{mT/mG}$ mice by crossing *Gli1*^{CreER} with the *R26*$^{mT/mG}$ reporter allele.[23] *R26*$^{mT/mG}$ is a cell membrane-targeted, two-color fluorescent Cre-reporter allele that expresses membrane-targeted Tomato (mT) prior to Cre-mediated excision and membrane-targeted GFP (mG) after excision.[23] Following tamoxifen injection in *Gli1*^{CreER}; *R26*$^{mT/mG}$ mice, we found that mGFP$^+$ cells were readily detected in the pericryptal stromal regions (Figure 3C). Immunofluorescence staining showed that all GFP$^+$ cells expressed vimentin, a pan-mesenchymal marker, and a subset of them were SMA positive (Figures 3C, 3E, 3F, and 3H), consistent with the idea that these Gli1+ cells are likely the mesenchymal progenitors that can differentiate into SMA-expressing myofibroblasts.[21]

We then calculated the percentage of vimentin$^+$ or SMA$^+$ cells in GFP$^+$ cells from the control *Gli1*^{CreER}; *R26*$^{mT/mG}$ mice and compared it with the percentage of vimentin$^+$ or SMA$^+$ cells in β-galactosidase$^+$ YAP5SA-expressing mutant cells in the mesenchymal overgrowth from *Gli1*^{CreER}; *R26*^{YAP5SA} mice (Figures 3C–3H). As expected, almost all control and YAP5SA-expressing cells expressed vimentin (Figures 3F–3H), whereas immunofluorescence staining of β-galactosidase and SMA in mesenchymal overgrowths showed very little co-expression in cells (Figures 3D and 3E). Together, these results suggested that, in addition to driving their proliferation, YAP/TAZ activation may also be able to alter the differentiation potential of the Gli1$^+$ mesenchymal progenitors.

Mesenchymal Hippo pathway regulates epithelial-mesenchymal crosstalk by promoting Wnt production

Gli1-expressing cells in the stem cell niche have been demonstrated to serve as one of the major sources of Wnt ligands and agonists, and they are essential for maintaining the epithelial stem cells.[21,24] We examined whether Hippo-YAP signaling regulates Wnt expression in the Gli1$^+$ cells. We measured the mRNA levels of Wnt ligands in the isolated intestinal mesenchymal cells with and without Hippo pathway inhibition. We found that Lats1/2 deletion or YAP5SA expression in Gli1$^+$ cells leads to higher levels of several Wnt ligands and agonists, including *Wnt2*, *Wnt2b*, *Wnt4*, *Rspo1*, and *Rspo3* (Figure 4A). Furthermore, we also performed qRT-PCR analysis of neuregulin 1, a key mesenchymal epidermal growth factor family ligand that plays a critical role in intestinal stem cell regeneration.[25] In addition, we also measured the mRNA levels of bone morphogenetic protein (BMP) family members, including *BMP2*, *BMP3*, *BMP5*, and *BMP7*, which have been reported to be expressed in the stem cell niche and regulate intestinal homeostasis.[26–28] We found that YAP/TAZ activation in Gli1+ cells did not significantly change the expression of these BMP factors (Figure S3A). Together, these data suggest an important role of mesenchymal Hippo-YAP signaling in regulating the production of stem cell niche factors, such as Wnt ligands and agonists.

Next, we focused on analyzing the effect of YAP/TAZ activation in Gli1$^+$ mesenchymal cells on epithelial Wnt pathway activity. We measured the expression levels of the well-established intestinal Wnt target genes, such as *Axin2* and *Cd44*. We found that Lats1/2 deletion or YAP5SA expression in Gli1$^+$ cells significantly increased the transcription of *Axin2* and *CD44* in the isolated intestinal epithelia from *Gli1*^{CreER}; *Lats1/2*$^{fL/fL}$ and *Gli1*^{CreER}; *R26*^{YAP5SA} mice following tamoxifen injection (Figure 4B). In the mesenchymal overgrowths detected in these mice, our IHC for CD44 and Sox9 (another epithelial Wnt target) showed that they were highly expressed in the epithelia adjacent to areas of mesenchymal overgrowths, and their expression levels are comparable to those in the crypt where Wnt signaling is normally activated (Figures 4C and 4D). We also examined whether mesenchymal YAP/TAZ activation will reciprocally regulate epithelial YAP/TAZ levels or activation of Src kinase, which is involved in YAP/TAZ-related mechano-transduction and tissue remodeling.[14] Our IHC for YAP/TAZ and

Figure 2. Hippo inhibition drives proliferation of niche-forming Gli1+ mesenchymal cells

(A) Histology of intestine and colon of control, *Gli1*^{CreER}; *Lats1/2* $^{fL/fL}$, and *Gli1*^{CreER}; *R26*^{YAP5SA} mice. Scale bar, 50 μm.

(B) Immunohistochemistry of YAP/TAZ and vimentin in mesenchymal overgrowths of *Gli1*^{CreER}; *Lats1/2* $^{fL/fL}$ mice. Inserts show staining in the area indicated by the dashed box. Scale bar, 50 μm.

(C) Immunohistochemistry of β-galactosidase (β-gal) and vimentin in mesenchymal overgrowths of *Gli1*^{CreER}; *R26*^{YAP5SA} mice. Inserts show staining in the area indicated by the dashed box. Scale bar, 50 μm.

(D) Immunofluorescence staining of YAP and vimentin in mesenchymal overgrowths of *Gli1*^{CreER}; *Lats1/2* $^{fL/fL}$ mice. Inserts show co-staining of YAP and vimentin in area indicated by dashed box. Scale bar, 50 μm.

(E) Immunohistochemistry of Ki67 staining in control intestine and mesenchymal overgrowths in *Gli1*^{CreER}; *Lats1/2* $^{fL/fL}$, *Gli1*^{CreER}; *R26*^{YAP5SA}; *Pdgfrβ*^{CreER}; *R26*^{YAP5SA} mice. Epithelia-mesenchyme boundaries are indicated by dashed lines. Me, mesenchyme; Ep, epithelia. Scale bar, 50 μm.

(F) Quantification of Ki67+ mesenchymal cells in control, *Gli1*^{CreER}; *Lats1/2* $^{fL/fL}$, and *Gli1*^{CreER}; *R26*^{YAP5SA}.

Data are mean ± SEM. $^{**}p < 0.01$, $^{***}p < 0.001$.

See also Figure S2.

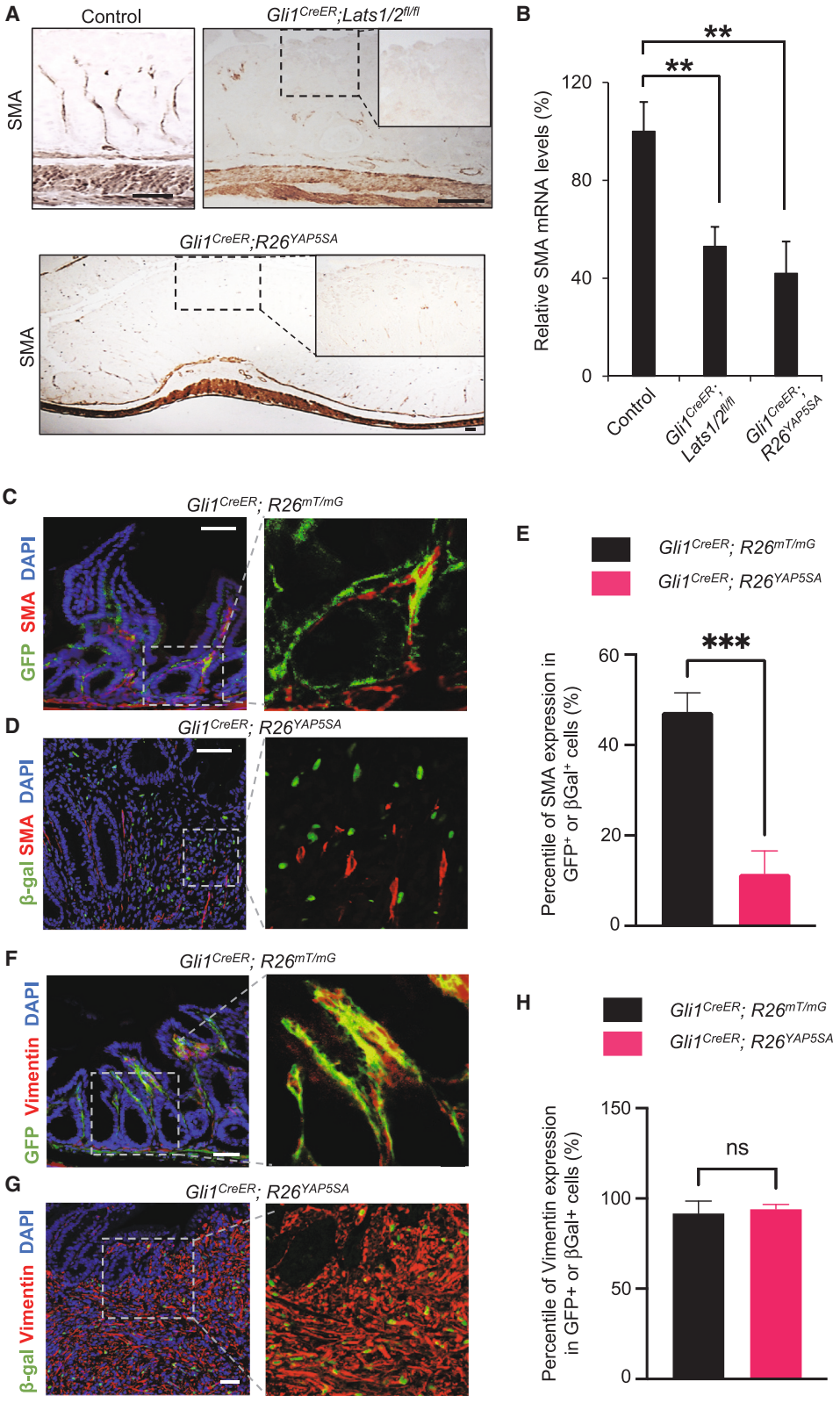

(legend on next page)

phosphor-Src (pSrc) showed that YAP/TAZ expression and Src activity did not significantly change in the epithelium. However, we did detect an increased level of pSrc staining in the mesenchyme (Figure S3B). Altogether, these data suggested that YAP/TAZ in Gli1$^+$ cells regulate the mesenchymal-epithelial crosstalk, at least in part by promoting mesenchymal Wnt ligand production leading to the elevated Wnt pathway in the epithelium.

Mesenchymal YAP activation facilitates epithelial regeneration following injury

Wnt signaling is crucial for stem cell renewal and regeneration following injury.[9,29–31] Since our data suggested that YAP activation within the mesenchymal compartment upregulates epithelial Wnt signaling (Figure 4), we hypothesized that mesenchymal YAP activation may expedite intestinal regeneration after injury.

To test this hypothesis, we utilized the intestinal injury model induced by the compound dextran sodium sulfate (DSS), regularly used *in vivo* to model colitis in mice.[32] DSS-induced injury is characterized by massive epithelial death, impairment of glandular architecture, and inflammation. We treated adult male animals with 2.5% DSS in their drinking water for 7 days, after which we replaced DSS water with regular water and allowed an additional 14 days for recovery (Figure 5A). Pathological evaluation revealed severe epithelial damage following 7 days of DSS treatment (day 7), in which the wounded areas exhibited an absence of glandular architecture and significantly less epithelial layer (Figure 5D). As recovery progressed, colonic mucosa exhibited wound-healing activities, including forming nascent crypts flanking the wound and epithelial differentiation at the wound's surface (Figure 5D). IHC staining of CD44 showed that the nascent crypts exhibited high Wnt pathway activation, and terminal differentiation of epithelial cells during recovery was revealed by the staining of Keratin 20 (Figure 5B). Interestingly, we noticed that mesenchymal expression of YAP/TAZ during injury and subsequent recovery was significantly higher than its levels in the mesenchyme before injury or after recovery (Figure 5B). Our qRT-PCR analysis of the mRNA levels of the YAP/TAZ target genes, *Ctgf* and *Ankrd1*, also showed that in addition to the epithelial compartment, the expression of Ctgf and Ankrd1 in the mesenchyme was markedly increased during injury and subsequent recovery period but reverted to the baseline level after recovery (Figure 5C). These data suggested an intriguing possibility that mesenchymal YAP/TAZ activity may potentially aid in epithelial regeneration.

Prior reports have also demonstrated that Wnt-secreting Gli1$^+$ mesenchymal cells not only serve as the essential niche for the intestinal stem cells at the normal state, but they are also markedly expanded after DSS treatment, indicating their involvement in epithelial recovery from injury.[21] Thus, to examine the effect of YAP activation in the Gli1$^+$ mesenchymal cells on intestinal regeneration, *Gli1*^{CreER}; *R26*^{YAP5SA} or *Gli1*^{CreER}; *R26*^{YAP5SA}; *R26*$^{mT/mG}$ mice were injected with tamoxifen to induce Cre recombination followed by DSS treatment. We found that, compared to control mice, *Gli1*^{CreER}; *R26*^{YAP5SA} mice showed significantly more robust recovery from injury. On day 7, nascent crypts and epithelial layers were absent in the wounded area in control mice but readily detected in *Gli1*^{CreER}; *R26*^{YAP5SA} mice (Figure 5B). During the recovery, epithelial regeneration was also more advanced in *Gli1*^{CreER}; *R26*^{YAP5SA} mice (Figure 5B). On Day 21 when colon homeostasis was restored in control mice, we detected mesenchymal overgrowths in *Gli1*^{CreER}; *R26*^{YAP5SA} mice, probably due to the persistent overexpression of YAP5SA in the Gli1$^+$ cells after recovery from injury (Figure 5B). Consistent with the previous report of the increase of Gli1$^+$ cells in DSS-treated mice,[21] we also found that YAP5SA-expressing/GFP+ mesenchymal cells in *Gli1*^{CreER}; *R26*^{YAP5SA}; *R26*$^{mT/mG}$ mice were present at the wounded areas, adjacent to the epithelia surrounding nascent colon crypts that expressed the Wnt target gene CD44 (Figure 5D). In addition, we histologically scored the severity of DSS-mediated injury (also referred to as colitis) in which inflammation, regeneration, crypt damage, and percent involvement were assessed in the colon for both control and mutant groups using a previously published grading system,[33] in which an individual total score ranges from 0 to 14 (least severe to most severe). Our analysis revealed that *Gli1*^{CreER}; *R26*^{YAP5SA} mutant colons were significantly less injured than control immediately following DSS treatment and during recovery (Figure 5E). Altogether, our data revealed mesenchymal YAP/TAZ upregulation during DSS-induced injury, and we showed that YAP activation in the niche-forming Gli1$^+$ mesenchymal cells promotes intestinal epithelial regeneration after injury.

DISCUSSION

The Hippo-YAP signaling pathway is intimately associated with intestinal homeostasis and tumorigenesis[5,6,8]; however, its precise function remains elusive. Much of the focus has been on Hippo-YAP signaling in the intestinal epithelium, and little is known about its function in the mesenchyme, a tissue layer that plays an essential role during intestinal development and homeostasis. Our prior study linked Hippo signaling to the embryonic gut mesenchyme, where YAP activation drives the

Figure 3. SMA downregulation in mesenchymal overgrowth induced by YAP/TAZ activation

(A) Immunohistochemistry of SMA in the control colon and overgrowths of *Gli1*^{CreER}; *Lats1/2*$^{fL/fL}$ and *Gli1*^{CreER}; *R26*^{YAP5SA} mice. Scale bar, 50 μm.

(B) Real-time PCR analysis of *SMA* mRNA levels in isolated *Gli1*^{CreER}; *Lats1/2* $^{fL/fL}$ and *Gli1*^{CreER}; *R26*^{YAP5SA} mesenchyme.

(C) Immunofluorescence staining of SMA and GFP in intestinal mesenchyme e of *Gli1*^{CreER}; *R26*$^{mT/mG}$ mice. Scale bar, 20 μm.

(D) Immunofluorescence staining of SMA and β-galactosidase (β-gal) in mesenchymal overgrowth of *Gli1*^{CreER}; *R26*^{YAP5SA} mice. Scale bar, 20 μm.

(E) Percentage of SMA expression in GFP$^+$ or β-gal$^+$ cells in control mesenchyme or overgrowths. Data are mean ± SEM. ***$p < 0.001$.

(F) Immunofluorescence staining of vimentin and GFP in intestinal mesenchyme of *Gli1*^{CreER}; *R26*$^{mT/mG}$ mice. Scale bar, 20 μm.

(G) Immunofluorescence staining of vimentin and β-galactosidase (β-gal) in mesenchymal overgrowth of *Gli1*^{CreER}; *R26*^{YAP5SA} mice. Scale bar, 50 μm.

(H) Percentage of vimentin expression in GFP$^+$ or β-gal$^+$ cells in control mesenchyme or overgrowths.

Data are mean ± SEM.

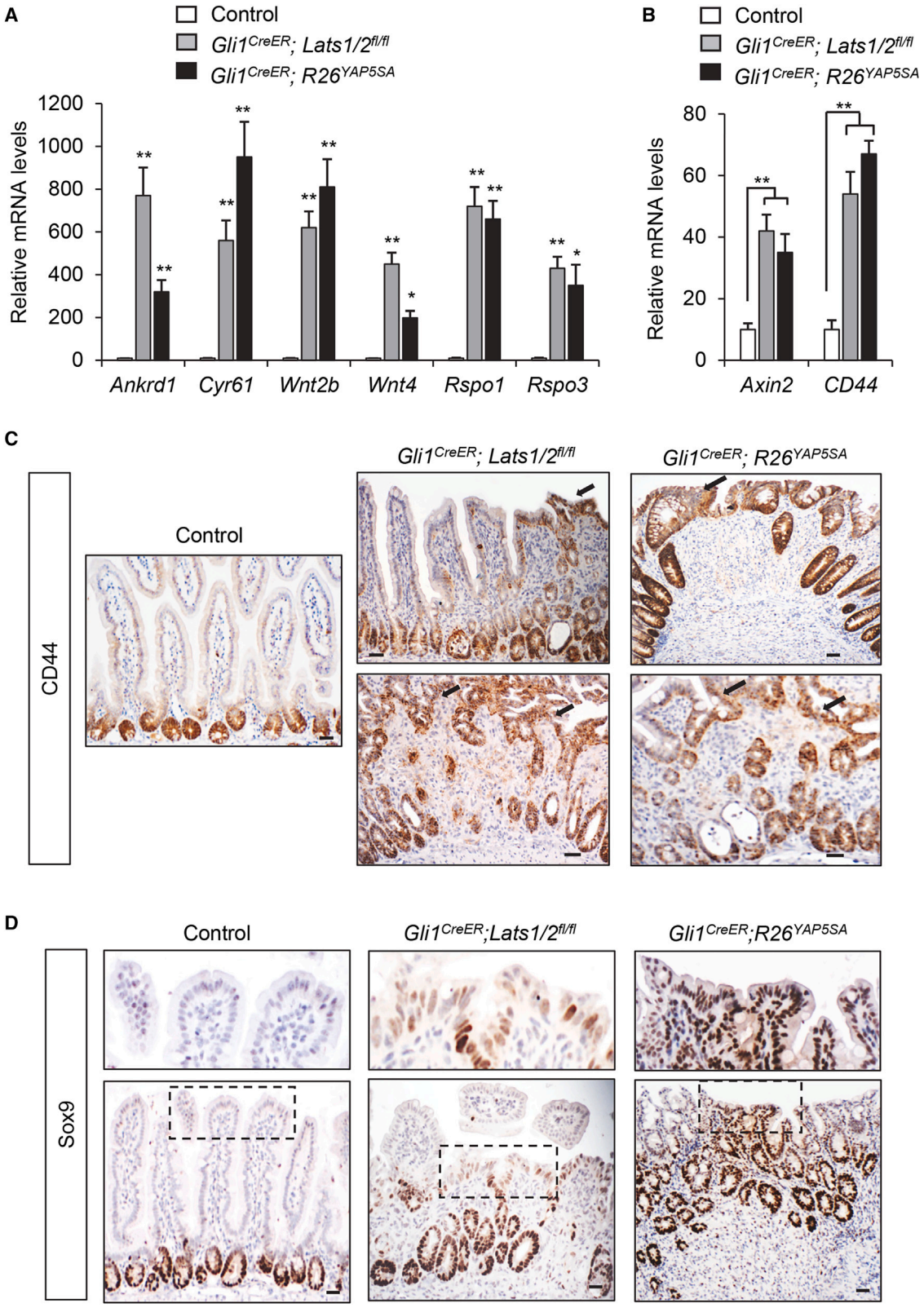

(legend on next page)

expansion of the mesenchymal progenitor populations.[17] Our work here focused on the role of Hippo-YAP signaling in adult intestinal mesenchymal cells. Recent reports have demonstrated that several populations of subepithelial mesenchymal cells, including the Gli1$^+$ progenitor cells, that form the essential Wnt-secreting niche to sustain intestinal stem cells.[21,34,35] However, how these cells are regulated is poorly unexplored. We identified Hippo/YAP as an important signaling pathway in the niche-forming mesenchymal cells that regulate intestinal epithelial-mesenchymal crosstalk.

Our result that Lats deletion or YAP activation in Gli1$^+$ cells induced mesenchymal overgrowth is in drastic contrast to the effect of Hippo pathway disruption in the smooth muscle layer. It is probably partly due to the baseline YAP/TAZ activity in different mesenchymal populations where YAP/TAZ is expressed much higher in the smooth muscle layer than in the subepithelial mesenchymal compartment (Figure 1). In fact, a recent report shows that deletion of YAP/TAZ in adult smooth muscle causes colonic pseudo-obstruction,[36] suggesting that the high baseline level of YAP/TAZ plays a functional role in the terminally differentiated smooth muscle layer. SMA downregulation in mesenchymal overgrowths induced by YAP/TAZ activation in Gli1$^+$ cells is also intriguing. We previously reported that YAP activation prevents SMA induction in the primitive embryonic mesenchymal progenitors,[17] and it is also consistent with the notion that Gli1$^+$ cells possess the characteristics of mesenchymal progenitors that are capable of differentiating into both SMA+ myofibroblasts or SMA− fibroblasts.[21] Thus, it is interesting to speculate that different wiring of the genetic or epigenetic circuitries in different mesenchymal populations may dictate the differential functional output responding to Hippo pathway disruption in these cell populations. Further investigation is needed to address these issues.

Most reports addressing the interaction between Wnt and Hippo-YAP signaling in the intestine have focused on the crosstalk of these two pathways in epithelial stem cells.[5–7,15,16,37] Our study identified the role of Hippo-YAP signaling in regulating Wnt ligand production in peri-cryptal mesenchymal cells. Thus, in addition to demonstrating the mesenchymal Hippo pathway as an important niche signal, our work uncovered another layer of the complex Hippo-Wnt functional interactions that involve both the epithelial and mesenchymal compartments during intestinal homeostasis.

Our results revealed that mesenchymal Hippo-YAP signaling regulates both normal homeostasis and intestinal pathogenesis. Our data showing that the YAP/TAZ level is markedly upregulated in the mesenchyme during intestinal injury and subsequent recovery are consistent with the idea that YAP/TAZ promotes the production of stem cell niche factors in the mesenchyme. Our result that stromal YAP promotes intestinal regeneration in a mouse model of colitis also links mesenchymal Hippo-YAP regulation to intestinal pathogenesis. Hippo signaling interacts with other signaling pathways, including receptor tyrosine kinases and transforming growth factor/BMP pathways, which have been shown to function in the mesenchymal niche during intestinal hemostasis.[2,3,28,38] It is interesting to explore how the interplays between Hippo-YAP and these signaling pathways in the mesenchyme may coordinate epithelial-mesenchymal crosstalk and how they can be exploited to design new therapeutic strategies for treating intestinal diseases and cancers.

Limitations of the study

Our studies have largely focused on the Gli1$^+$ intestinal mesenchymal cells. The potential role of Hippo-YAP signaling in other niche-forming pericryptal cell populations needs to be further investigated. In addition, we used a mouse model of colitis, which may not fully recapitulate the pathogenesis of human disease.

RESOURCE AVAILABILITY

Lead contact

Further information and requests should be directed to and will be fulfilled by the lead contact, Junhao Mao (Junhao.mao@umassmed.edu).

Materials availability

This study did not generate new unique reagents.

Data and code availability

- All data reported in this article will be shared by the lead contact upon request.
- This article does not report the original code.
- Any additional information required to reanalyze the data reported in this paper is available from the lead contact upon request.

ACKNOWLEDGMENTS

This work was supported by grants from the National Institutes of Health, R01DK127180 and R01DK127207 to J.M. and R01CA238270 and R01DK107651 to X.W. We also thank the members of the Mao lab for helpful discussions and comments on the manuscript.

AUTHOR CONTRIBUTIONS

K.D. and J.M. conceived and designed the study. K.D., A.S., X.C., J.L.C., Z.T., H.L., and L.J.Z. acquired the data. K.D., A.S., X.C., and J.M. analyzed and interpreted the data. Y.T.I., X.W., and J.M. were responsible for fund acquisition. K.D., X.C., and J.M. wrote the manuscript. J.M. supervised the study.

Figure 4. Mesenchymal Hippo signaling affects epithelial-mesenchymal crosstalk by regulating Wnt production

(A) Real-time PCR analysis of YAP targets *Ankrd1* and *Cyr61* and Wnt ligands/agonists *Wnt2b, Wnt4, Rspo1, and Rspo3* mRNA levels in isolated *Gli1^{CreER};Lats1/2$^{fL/fL}$* and *Gli1^{CreER};R26^{YAP5SA}* mesenchyme. Data are mean ± SEM, $^*p < 0.05$, $^{**}p < 0.01$.

(B) Real-time PCR analysis of intestinal Wnt targets *Axin2* and *CD44* mRNA levels in isolated *Gli1^{CreER}; Lats1/2 $^{fL/fL}$* and *Gli1^{CreER};R26^{YAP5SA}* intestinal epithelia. Data are mean ± SEM, $^{**}p < 0.01$.

(C) Immunohistochemistry of CD44 in control, *Gli1^{CreER};Lats1/2$^{fL/fL}$*, and *Gli1^{CreER};R26^{YAP5SA}* epithelia. Arrows point to CD44 expression in the epithelia adjacent to mesenchymal overgrowths. Scale bar, 20 μm.

(D) Immunohistochemistry of SOX9 in control, *Gli1^{CreER};Lats1/2$^{fL/fL}$*, and *Gli1^{CreER};R26^{YAP5SA}* epithelia. Upper panels show areas indicated by dashed boxes. Scale bar, 20 μm.

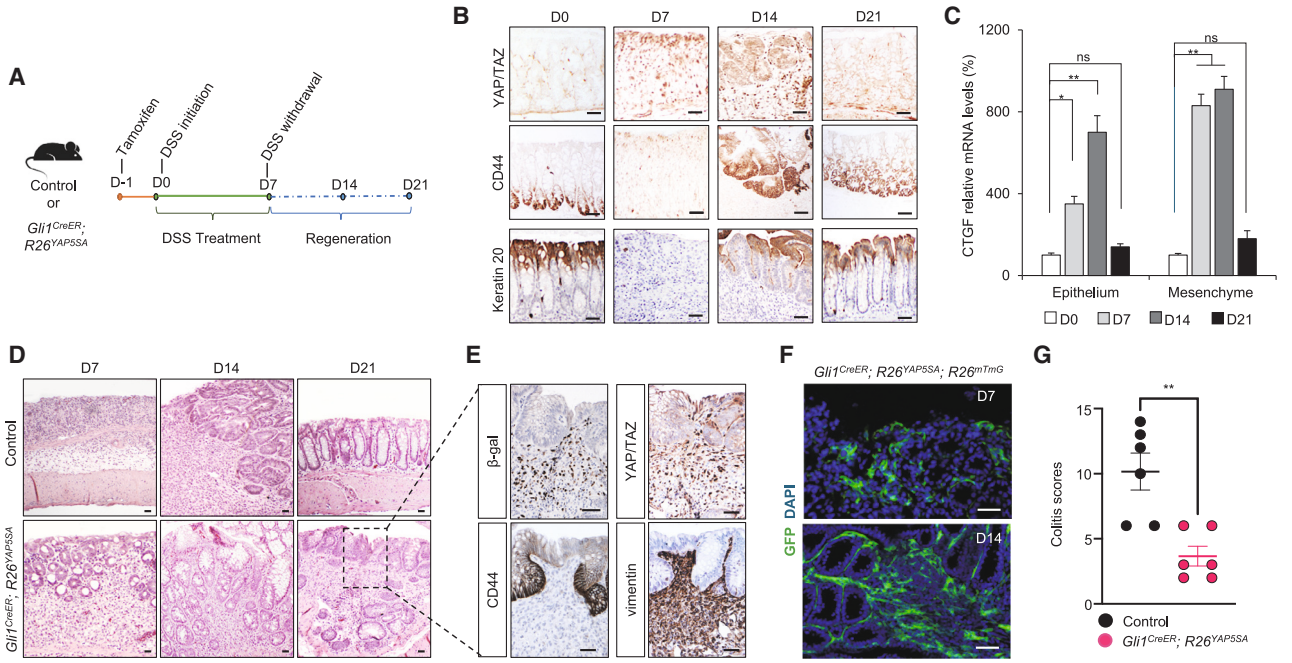

Figure 5. Mesenchymal YAP/TAZ Activation promotes intestinal regeneration induced by DSS treatment

(A) Schematic of experimental design, indicating tamoxifen treatment, duration of DSS treatment, and recovery.

(B) Immunohistochemistry of YAP/TAZ, CD44, and Keratin-20 in control intestine during DSS treatment and subsequent recovery at time points day 0 (D0), day 7 (D7), day 14 (D14), and day 21 (D21). Scale bar, 20 μm.

(C) Real-time PCR analysis of *Ctgf* and *Ankrd1* mRNA levels in control animals at different time points following DSS treatment. Data are mean ± SEM, $*p < 0.05$, $**p < 0.01$, ns: not significant.

See also Figure S1.

(D) Histology of control and $Gli1^{CreER}; R26^{YAP5SA}$ colon at time points D7, D14, and D21 of recovery. Scale bar, 20 μm.

(E) Immunohistochemistry of β-galactosidase (β-gal), YAP/TAZ, CD44, and vimentin in areas of mesenchymal overgrowth in $Gli1^{CreER}; R26^{YAP5SA}$ colon at D21. Scale bar, 20 μm.

(F) GFP signal in $Gli1^{CreER}; R26^{YAP5SA}; R26^{mT/mG}$ colon at D7 and D14 during regeneration. Scale bar, 50 μm.

(G) Colitis scoring of control and $Gli1^{CreER}; R26^{YAP5SA}$ colon. Data are mean ± SEM, $**p < 0.01$.

DECLARATION OF INTERESTS

X.W. has a financial interest in Tasca Therapeutics, which is developing small-molecule modulators of TEAD palmitoylation and transcription factors. X.W.'s interests were reviewed and are managed by Mass General Hospital and Mass General Brigham in accordance with their conflict of interest polices.

STAR★METHODS

Detailed methods are provided in the online version of this paper and include the following:

- KEY RESOURCES TABLE
- EXPERIMENTAL MODEL AND SUBJECT PARTICIPANT DETAILS
- METHOD DETAILS
  - Tissue Collection and Histology
  - Immunohistochemistry and immunofluorescence
  - Western blot analysis
  - Quantitative real-time PCR
- QUANTIFICATION AND STATISTICAL ANALYSIS

SUPPLEMENTAL INFORMATION

Supplemental information can be found online at https://doi.org/10.1016/j.isci.2025.111847.

Received: May 9, 2024
Revised: October 16, 2024
Accepted: January 16, 2025
Published: January 20, 2025

REFERENCES

1. Kedinger, M., Duluc, I., Fritsch, C., Lorentz, O., Plateroti, M., and Freund, J.N. (1998). Intestinal epithelial-mesenchymal cell interactions. Ann. N. Y. Acad. Sci. *859*, 1–17. https://doi.org/10.1111/j.1749-6632.1998.tb11107.x.

2. Kolev, H.M., and Kaestner, K.H. (2023). Mammalian Intestinal Development and Differentiation-The State of the Art. Cell. Mol. Gastroenterol. Hepatol. *16*, 809–821. https://doi.org/10.1016/j.jcmgh.2023.07.011.

3. Brugger, M.D., and Basler, K. (2023). The diverse nature of intestinal fibroblasts in development, homeostasis, and disease. Trends Cell Biol. *33*, 834–849. https://doi.org/10.1016/j.tcb.2023.03.007.

4. Halder, G., and Camargo, F.D. (2013). The hippo tumor suppressor network: from organ size control to stem cells and cancer. Cancer Res. *73*, 6389–6392. https://doi.org/10.1158/0008-5472.CAN-13-2392.

5. Hong, A.W., Meng, Z., and Guan, K.L. (2016). The Hippo pathway in intestinal regeneration and disease. Nat. Rev. Gastroenterol. Hepatol. *13*, 324–337. https://doi.org/10.1038/nrgastro.2016.59.

6. Gregorieff, A., and Wrana, J.L. (2017). Hippo signalling in intestinal regeneration and cancer. Curr. Opin. Cell Biol. *48*, 17–25. https://doi.org/10.1016/j.ceb.2017.04.005.

7. Zanconato, F., Cordenonsi, M., and Piccolo, S. (2016). YAP/TAZ at the Roots of Cancer. Cancer Cell *29*, 783–803. https://doi.org/10.1016/j.ccell.2016.05.005.

8. Zheng, Y., and Pan, D. (2019). The Hippo Signaling Pathway in Development and Disease. Dev. Cell *50*, 264–282. https://doi.org/10.1016/j.devcel.2019.06.003.

9. Ma, S., Meng, Z., Chen, R., and Guan, K.L. (2019). The Hippo Pathway: Biology and Pathophysiology. Annu. Rev. Biochem. *88*, 577–604. https://doi.org/10.1146/annurev-biochem-013118-111829.

10. Piccolo, S., Panciera, T., Contessotto, P., and Cordenonsi, M. (2023). YAP/TAZ as master regulators in cancer: modulation, function and therapeutic approaches. Nat. Can. (Ott.) *4*, 9–26. https://doi.org/10.1038/s43018-022-00473-z.

11. Barry, E.R., Morikawa, T., Butler, B.L., Shrestha, K., de la Rosa, R., Yan, K.S., Fuchs, C.S., Magness, S.T., Smits, R., Ogino, S., et al. (2013). Restriction of intestinal stem cell expansion and the regenerative response by YAP. Nature *493*, 106–110. https://doi.org/10.1038/nature11693.

12. Cai, J., Zhang, N., Zheng, Y., de Wilde, R.F., Maitra, A., and Pan, D. (2010). The Hippo signaling pathway restricts the oncogenic potential of an intestinal regeneration program. Genes Dev. *24*, 2383–2388. https://doi.org/10.1101/gad.1978810.

13. Gregorieff, A., Liu, Y., Inanlou, M.R., Khomchuk, Y., and Wrana, J.L. (2015). Yap-dependent reprogramming of Lgr5(+) stem cells drives intestinal regeneration and cancer. Nature *526*, 715–718. https://doi.org/10.1038/nature15382.

14. Yui, S., Azzolin, L., Maimets, M., Pedersen, M.T., Fordham, R.P., Hansen, S.L., Larsen, H.L., Guiu, J., Alves, M.R.P., Rundsten, C.F., et al. (2018). YAP/TAZ-Dependent Reprogramming of Colonic Epithelium Links ECM Remodeling to Tissue Regeneration. Cell Stem Cell *22*, 35–49.e7. https://doi.org/10.1016/j.stem.2017.11.001.

15. Li, Q., Sun, Y., Jarugumilli, G.K., Liu, S., Dang, K., Cotton, J.L., Xiol, J., Chan, P.Y., DeRan, M., Ma, L., et al. (2020). Lats1/2 Sustain Intestinal Stem Cells and Wnt Activation through TEAD-Dependent and Independent Transcription. Cell Stem Cell *26*, 675–692.e8. https://doi.org/10.1016/j.stem.2020.03.002.

16. Cheung, P., Xiol, J., Dill, M.T., Yuan, W.C., Panero, R., Roper, J., Osorio, F.G., Maglic, D., Li, Q., Gurung, B., et al. (2020). Regenerative Reprogramming of the Intestinal Stem Cell State via Hippo Signaling Suppresses Metastatic Colorectal Cancer. Cell Stem Cell *27*, 590–604.e9. https://doi.org/10.1016/j.stem.2020.07.003.

17. Cotton, J.L., Li, Q., Ma, L., Park, J.S., Wang, J., Ou, J., Zhu, L.J., Ip, Y.T., Johnson, R.L., and Mao, J. (2017). YAP/TAZ and Hedgehog Coordinate Growth and Patterning in Gastrointestinal Mesenchyme. Dev. Cell *43*, 35–47.e4. https://doi.org/10.1016/j.devcel.2017.08.019.

18. Yi, J., Lu, L., Yanger, K., Wang, W., Sohn, B.H., Stanger, B.Z., Zhang, M., Martin, J.F., Ajani, J.A., Chen, J., et al. (2016). Large tumor suppressor homologs 1 and 2 regulate mouse liver progenitor cell proliferation and maturation through antagonism of the coactivators YAP and TAZ. Hepatology *64*, 1757–1772. https://doi.org/10.1002/hep.28768.

19. Wirth, A., Benyó, Z., Lukasova, M., Leutgeb, B., Wettschureck, N., Gorbey, S., Orsy, P., Horváth, B., Maser-Gluth, C., Greiner, E., et al. (2008). G12-G13-LARG-mediated signaling in vascular smooth muscle is required for salt-induced hypertension. Nat. Med. *14*, 64–68. https://doi.org/10.1038/nm1666.

20. Zhao, B., Wei, X., Li, W., Udan, R.S., Yang, Q., Kim, J., Xie, J., Ikenoue, T., Yu, J., Li, L., et al. (2007). Inactivation of YAP oncoprotein by the Hippo pathway is involved in cell contact inhibition and tissue growth control. Genes Dev. *21*, 2747–2761. https://doi.org/10.1101/gad.1602907.

21. Degirmenci, B., Valenta, T., Dimitrieva, S., Hausmann, G., and Basler, K. (2018). GLI1-expressing mesenchymal cells form the essential Wnt-secreting niche for colon stem cells. Nature *558*, 449–453. https://doi.org/10.1038/s41586-018-0190-3.

22. Ahn, S., and Joyner, A.L. (2005). In vivo analysis of quiescent adult neural stem cells responding to Sonic hedgehog. Nature *437*, 894–897. https://doi.org/10.1038/nature03994.

23. Muzumdar, M.D., Tasic, B., Miyamichi, K., Li, L., and Luo, L. (2007). A global double-fluorescent Cre reporter mouse. Genesis *45*, 593–605. https://doi.org/10.1002/dvg.20335.

24. Valenta, T., Degirmenci, B., Moor, A.E., Herr, P., Zimmerli, D., Moor, M.B., Hausmann, G., Cantù, C., Aguet, M., and Basler, K. (2016). Wnt Ligands Secreted by Subepithelial Mesenchymal Cells Are Essential for the Survival of Intestinal Stem Cells and Gut Homeostasis. Cell Rep. *15*, 911–918. https://doi.org/10.1016/j.celrep.2016.03.088.

25. Jarde, T., Chan, W.H., Rossello, F.J., Kaur Kahlon, T., Theocharous, M., Kurian Arackal, T., Flores, T., Giraud, M., Richards, E., Chan, E., et al. (2020). Mesenchymal Niche-Derived Neuregulin-1 Drives Intestinal Stem Cell Proliferation and Regeneration of Damaged Epithelium. Cell Stem Cell *27*, 646–662.e7. https://doi.org/10.1016/j.stem.2020.06.021.

26. He, X.C., Zhang, J., Tong, W.G., Tawfik, O., Ross, J., Scoville, D.H., Tian, Q., Zeng, X., He, X., Wiedemann, L.M., et al. (2004). BMP signaling inhibits intestinal stem cell self-renewal through suppression of Wnt-beta-catenin signaling. Nat. Genet. *36*, 1117–1121. https://doi.org/10.1038/ng1430.

27. Brugger, M.D., Valenta, T., Fazilaty, H., Hausmann, G., and Basler, K. (2020). Distinct populations of crypt-associated fibroblasts act as signaling hubs to control colon homeostasis. PLoS Biol. *18*, e3001032. https://doi.org/10.1371/journal.pbio.3001032.

28. McCarthy, N., Kraiczy, J., and Shivdasani, R.A. (2020). Cellular and molecular architecture of the intestinal stem cell niche. Nat. Cell Biol. *22*, 1033–1041. https://doi.org/10.1038/s41556-020-0567-z.

29. Kretzschmar, K., and Clevers, H. (2017). Wnt/beta-catenin signaling in adult mammalian epithelial stem cells. Dev. Biol. *428*, 273–282. https://doi.org/10.1016/j.ydbio.2017.05.015.

30. Nusse, R., and Clevers, H. (2017). Wnt/beta-Catenin Signaling, Disease, and Emerging Therapeutic Modalities. Cell *169*, 985–999. https://doi.org/10.1016/j.cell.2017.05.016.

31. Mah, A.T., Yan, K.S., and Kuo, C.J. (2016). Wnt pathway regulation of intestinal stem cells. J. Physiol. *594*, 4837–4847. https://doi.org/10.1113/JP271754.

32. Chassaing, B., Aitken, J.D., Malleshappa, M., and Vijay-Kumar, M. (2014). Dextran sulfate sodium (DSS)-induced colitis in mice. Curr. Protoc. Im. *104*, 15.25.1–15.25.14. https://doi.org/10.1002/0471142735.im1525s104.

33. Dieleman, L.A., Palmen, M.J., Akol, H., Bloemena, E., Peña, A.S., Meuwissen, S.G., and Van Rees, E.P. (1998). Chronic experimental colitis induced by dextran sulphate sodium (DSS) is characterized by Th1 and Th2 cytokines. Clin. Exp. Immunol. *114*, 385–391. https://doi.org/10.1046/j.1365-2249.1998.00728.x.

34. Greicius, G., Kabiri, Z., Sigmundsson, K., Liang, C., Bunte, R., Singh, M.K., and Virshup, D.M. (2018). PDGFRalpha(+) pericryptal stromal cells are the critical source of Wnts and RSPO3 for murine intestinal stem cells *in vivo*. Proc. Natl. Acad. Sci. USA *115*, E3173–E3181. https://doi.org/10.1073/pnas.1713510115.

35. Shoshkes-Carmel, M., Wang, Y.J., Wangensteen, K.J., Tóth, B., Kondo, A., Massasa, E.E., Itzkovitz, S., and Kaestner, K.H. (2018). Subepithelial telocytes are an important source of Wnts that supports intestinal crypts. Nature *557*, 242–246. https://doi.org/10.1038/s41586-018-0084-4.

36. Daoud, F., Holmberg, J., Alajbegovic, A., Grossi, M., Rippe, C., Swärd, K., and Albinsson, S. (2021). Inducible Deletion of YAP and TAZ in Adult Mouse Smooth Muscle Causes Rapid and Lethal Colonic Pseudo-Obstruction. Cell. Mol. Gastroenterol. Hepatol. *11*, 623–637. https://doi.org/10.1016/j.jcmgh.2020.09.014.

37. Cai, J., Maitra, A., Anders, R.A., Taketo, M.M., and Pan, D. (2015). beta-Catenin destruction complex-independent regulation of Hippo-YAP

signaling by APC in intestinal tumorigenesis. Genes Dev. *29*, 1493–1506. https://doi.org/10.1101/gad.264515.115.

38. McCarthy, N., Manieri, E., Storm, E.E., Saadatpour, A., Luoma, A.M., Kapoor, V.N., Madha, S., Gaynor, L.T., Cox, C., Keerthivasan, S., et al. (2020). Distinct Mesenchymal Cell Populations Generate the Essential Intestinal BMP Signaling Gradient. Cell Stem Cell *26*, 391–402.e5. https://doi.org/10.1016/j.stem.2020.01.008.

39. Ahn, S., and Joyner, A.L. (2004). Dynamic changes in the response of cells to positive hedgehog signaling during mouse limb patterning. Cell *118*, 505–516. https://doi.org/10.1016/j.cell.2004.07.023.

40. Schindelin, J., Arganda-Carreras, I., Frise, E., Kaynig, V., Longair, M., Pietzsch, T., Preibisch, S., Rueden, C., Saalfeld, S., Schmid, B., et al. (2012). Fiji: an open-source platform for biological-image analysis. Nat. Methods *9*, 676–682. https://doi.org/10.1038/nmeth.2019.

STAR★METHODS

KEY RESOURCES TABLE

REAGENT or RESOURCE	SOURCE	IDENTIFIER
Antibodies		
Rabbit anti-YAP/TAZ	Cell Signaling	Cat# 8418, RRID: AB_10950494
Rabbit anti-YAP	Cell Signaling	Cat# 14074, RRID: AB_2650491
Rabbit anti-Ki67	Abcam	Cat# ab15580, RRID: AB_443209
Rat anti-CD44	Thermo Fisher Scientific	Cat# 14-0441-82, RRID: AB_467246
Rabbit anti-α-SMA	Abcam	Cat# ab5694, RRID: AB_2223021
Rabbit anti-Vimentin	Cell Signaling Technology	Cat# 5741, RRID: AB_10695459
Rabbit anti-Keratin 20	Cell Signaling Technology	Cat # 13063, RRID: AB_2798106
Chicken anti-β-Galactosidase	Abcam	Cat # ab9361, RRID: AB_307210
Rabbit anti-Desmin	Abcam	Cat # ab15200, RRID: AB_301744
Rat anti-GAPDH	BioLegend	Cat# 607901, RRID: AB_2734502
Rabbit anti-Cre Recombinase	Cell Signaling Technology	Cat# 15036, RRID: AB_2798694
Rabbit anti-Lysozyme	Novus	Cat# NBP1-95509, RRID: AB_11037059
Mouse anti-PCNA	Abcam	Cat# ab29, RRID: AB_303394
Rabbit anti-SOX9	Abcam	Cat# ab185230, RRID: AB_2715497
Biotinylated goat anti-chicken IgG	Vector Laboratories	Cat# BA-9010, RRID: AB_2336114
Biotinylated goat anti-rabbit IgG	Vector Laboratories	Cat # BA-1000, RRID: AB_2313606
Biotinylated goat anti-mouse IgG	Vector Laboratories	Cat # BA-9200, RRID: AB_2336171
Biotinylated goat anti-rat IgG	Vector Laboratories	Cat# BA-9400, RRID: AB_2336202
Alexa Fluor 488, goat anti-rabbit	Invitrogen	Cat# A-11008, RRID: AB_143165
Alexa Fluor 568, goat anti-rabbit	Invitrogen	Cat# A-11036, RRID: AB_10563566
Alexa Fluor 647, goat anti-chicken	Invitrogen	Cat# A-21449, RRID: AB_2535866
HRP conjugated goat anti-rabbit	Jackson ImmunoResearch	Cat# 111-035-144, RRID: AB_2307391
HRP conjugated goat anti-rat	Jackson ImmunoResearch	Cat# 112-035-143 RRID: AB_2338138
Rabbit anti-phospho-SRC	Invitrogen	Cat# 44660G, RRID: AB_2533714
Chemicals, peptides, and recombinant proteins		
Dextran Sodium Sulfate Salt (DSS), Colitis Grade (36,000-50,000 MW)	MP Biomedicals	0216011010
Trizol reagent	Invitrogen	Cat# 15596026
Tamoxifen	Sigma	Cat# T5648
Critical commercial assays		
Vectastain Elite ABC Kit	Vector Laboratories	PK-6100
Immpact® DAB Substrate, Peroxidase (HRP)	Vector Laboratories	SK-4105
SignalStain® Citrate Unmasking Solution (10X)	Cell Signaling	14746
AzuraQuant cDNA Synthesis Kit	Azura Genomics	AZ-1995
AzuraQuant Green Fast qPCR Mix Lo Rox	Azura Genomics	AZ-2105
Alcian Blue Reagent	Electron Microscopy Sciences	26026-13
Experimental models: Organisms/strains		
Mouse: *Myh11*^{CreER}: B6.FVB-Tg(Myh11-icre/ERT2)1Soff/J	(Wirth et al., 2008)	JAX: 019079, RRID:IMSR_JAX:019079
Mouse: *Gli1*^{CreER}: *Gli1*$^{tm3(cre/ERT2)Alj}$/J	Ahn and Joyner[39]	JAX: 007913, RRID:IMSR_JAX:007913
Mouse: *Lats1*$^{fl/fl}$: *Lats1*$^{tm1.1Jfm}$/RjoJ	(Yi et al., 2016)	JAX: 024941, RRID:IMSR_JAX:024941
Mouse: *Lats2*$^{fl/fl}$: *Lats2*$^{tm1.1Jfm}$/RjoJ	(Yi et al., 2016)	JAX: 025428, RRID:IMSR_JAX:025428
Mouse: B6.129(Cg)-*Gt(ROSA)26Sor*$^{tm4(ACTB-tdTomato,-EGFP)Luo}$/J	(Muzumdar et al., 2007)	JAX: 007676, RRID:IMSR_JAX:007676
Mouse: *R26*^{YAP5SA}	(Cotton et al., 2017)	N/A

(*Continued on next page*)

Continued		
REAGENT or RESOURCE	SOURCE	IDENTIFIER
Oligonucleotides		
Primers for qRT-PCR (Wnt ligands)	Degirmenci et al.[21]	See below
Primers for qRT-PCR (YAP targets)	Li et al.[15]	See below
Software and algorithms		
GraphPad Prism 9	GraphPad	https://www.graphpad.com/, RRID:SCR_002798
Fiji (ImageJ)	Schindelin et al.[40]	https://fiji.sc/, RRID:SCR_002285

EXPERIMENTAL MODEL AND SUBJECT PARTICIPANT DETAILS

Gli1^{CreER},[39] *Myh11*^{CreER},[19] *Lats1*^{flox} and *Lats2*^{flox},[18] and *R26*$^{mT/mG}$[23] mice were obtained from the Jackson laboratory. *R26*^{YAP5SA} mice were described previously [17]Cre activation of the inducible Cre lines was achieved by one-time intraperitoneal injection of 120mg/kg Tamoxifen (Sigma) into one-month-old mice of both sexes with appropriate genotypes. For DSS-colitis model, *Gli1*^{CreERA}; *R26*$^{mT/mG}$ control and *Gli1*^{CreER}; *R26*^{YAP5SA}; *R26*$^{mT/mG}$ mutant animals of 8 weeks of age or older of both sexes were induced with one single dose of 300 mg/kg tamoxifen one day prior to treatment with 2.5% w/v dextran sodium sulfate (DSS) in autoclaved drinking water. Animals were treated for 7 consecutive days before regular drinking water was re-introduced. Animals from each group were sacrificed at pre-determined time points: Immediately following DSS treatment (D7), 7 days following DSS treatment (D14), and 14 days following DSS treatment (D21). The colon was harvested and prepared for both paraffin and OCT embedding and stained with hematoxylin and eosin as described under "tissue collection and histology." Colitis injury was histologically scored using H&E paraffin sections and criteria previously published.[33] All animal use protocols were reviewed and approved by The University of Massachusetts Chan Medical School Institutional Animal Care and Use Committee.

METHOD DETAILS

Tissue Collection and Histology

Following euthanasia, mouse intestinal or polyp tissue was dissected and fixed in 10% Neutral Buffered Formalin (NBF) at 4°C overnight. For paraffin sections, tissue was dehydrated, embedded in paraffin, and sectioned at 6 μm. For frozen sections, tissue was dehydrated in 30% sucrose overnight at 4°C, embedded in OCT, and sectioned at 12 μm. Paraffin sections were stained using standard hematoxylin & eosin reagents. For intestinal epithelium and mesenchyme isolation, mouse small intestinal tissues at different postnatal stages are dissected and washed in cold PBS, before transferring to PBS containing 3mM EDTA for rotation at 4°C for 30 mins. After vigorous shaking for 2 mins, the epithelial tissues are collected in the supernatant, while the remaining mesenchymal tissues are washed and incubated with the digestion buffer containing Collagenase XI and Dispase at 37°C for 30min, and the samples are then subjected to western blot and quantitative real-time PCR analyses.

Immunohistochemistry and immunofluorescence

For immunohistochemistry (IHC), sections were deparaffinized and rehydrated before undergoing heat-induced antigen retrieval in 10mM sodium citrate buffer (pH 6.0) for 30 minutes. Slides were blocked for endogenous peroxidase for 20 minutes, then blocked for 1 hour in 5% BSA, 1% goat serum, 0.1% Tween-20 buffer in PBS, and incubated overnight at 4°C in primary antibody diluted in blocking buffer or SignalStain® Antibody Diluent (Cell Signaling). Slides were incubated in biotinylated secondary antibodies for 1 hour at room temperature and signal was detected using the Vectastain Elite ABC kit (Vector Laboratories). For immunofluorescence (IF), cells or tissue sections were fixed by 4% paraformaldehyde for 5 minutes, blocked for 1 hour and incubated overnight at 4°C in primary antibody diluted in blocking buffer. Slides were then incubated for 1 hour at room temperature in Alexa Fluor-conjugated secondary antibodies (Invitrogen) at 1:500 dilution in blocking buffer and mounted using mounting media with DAPI (EMS).

Primary antibodies used for IHC/IF were YAP/TAZ (Cell Signaling), Vimentin (Cell Signaling), Ki67 (Abcam), CD44 (eBioscience), β-galactosidase (Abcam), Desmin (Abcam), SOX9 (Abcam), Keratin 20 (Cell Signaling), lysozyme (Novus), PCNA (Abcam), Cre recombinase (Cell signaling), and α-smooth muscle actin (SMA) (Abcam).

Western blot analysis

Freshly isolated mouse tissue was lysed in lysis buffer (50 mM Tris-HCl, pH 7.4, 150 mM NaCl, 0.5 mM EDTA, 1% Triton X-100, phosphatase inhibitor cocktail, complete EDTA-free protease inhibitors cocktail) for 30min at 4°C. The supernatants of the extracts were then used for western blot following the protocols described previously.[17] The primary antibodies used in these assays were YAP/TAZ (Cell Signaling) and GAPDH (Bethyl). HRP-conjugated Secondary antibodies were obtained from Jackson Laboratories.

Quantitative real-time PCR

Total RNA was isolated using Trizol reagent (Invitrogen). cDNA synthesis was performed using AzuraQuant^{TM} cDNA synthesis kit (Azura Genomics), and the number of transcripts were quantified using AzuraQuant^{TM} Green Fast qPCR Mix Lo-Rox (Azura Genomics), with the respective oligonucleotides: (CTGF forward: TGTGCACTGCCAAAGATGGTGCAC, reverse: TGGGCAGGCGCAC GTCCATG; Cyr61 forward: GAGGCTTCCTGTCTTTGGCAC, reverse: ACTCTGGGTTGTCATTGGTAAC; ANKRD1 forward: GGAAC AACGGAAAAGCGAGAA, reverse: GAAACCTCGGCACATCCACA; Nrg1 Forward: AACCCACCACCAGAGAATGT, reverse: TGGCA ACGATCACCAGTAAA; BPM2 forward: ACCCCCAGCAAGGACGTCGT, reverse: AAGAAGCGCCGGGCCGTTTT; BMP3 forward: AGCAGTGGGTCGAACCTCGGA, reverse: ACCCCCACCGCTCGCACTAT; BMP5 forward: ATCAGGACCCCTCCAGGATGCC, reverse: TGATCCAGTCCTGCCATCCCAGATC; BMP7 forward: CAAGCAGCGCAGCCAGAATCG, reverse: CAATGATCCAGTCCT GCCAGCCAA) in QuantStudio 6 Flex Real-Time PCR Systems (Applied Biosystems). All qPCR experiments were conducted in biological triplicates, error bars represent mean ± standard error mean, and Student's t-test was used to generate p-values (* = p value <0.05; ** = p value <0.01; *** = p value <0.001).

QUANTIFICATION AND STATISTICAL ANALYSIS

No statistical method was used to predetermine the sample size. The experiments were not randomized. For biochemical experiments we performed the experiments at least three independent times. Experiments for which we showed representative images were performed successfully at least 3 independent times. No samples or animals were excluded from the analysis. The investigators were not blinded to allocation during experiments and outcome assessment. Student's t-test was used to generate p-values * = p value <0.05; ** = p value <0.01; *** = p value <0.001). The variance was similar between the groups that we compared.